Journal of Sol-Gel Science and Technology
https://doi.org/10.1007/s10971-023-06156-0

ORIGINAL PAPER: MODELLING, COMPUTATIONAL TOOLS AND THEORETICAL STUDIES OF SOL-GEL AND HYBRID MATERIALS

On the origin of power-scaling exponents in silica aerogels

Shivangi Aney[1] · Prakul Pandit[1] · Lorenz Ratke[1] · Barbara Milow[1,2] · Ameya Rege[1,3]

Received: 4 March 2023 / Accepted: 31 May 2023

Abstract

The macroscopic properties of open-porous cellular materials hinge upon the microscopic skeletal architecture and features of the material. Typically, bulk material properties, viz. the elastic modulus, strength of the material, thermal conductivity, and acoustic velocity, of such porous materials are expressed in terms of power-scaling laws against their density. In particular, the relation between the elastic modulus and the density has been intensively investigated. While the Gibson and Ashby model predicts an exponent of 2 for ideally connected foam-like open-cellular solids, the exponent is found to lie between 3 and 4 for silica aerogels. In this paper, we investigate the origins of this scaling exponent. Particularly, the effect of the pearl-necklace-like skeletal features of the pore walls and that of the random spatial arrangement is extensively computationally studied. It is shown that the latter is the driving factor in dictating the scaling exponent and the rest of the features play a negligible or no role in quantifying the scaling exponent.

Graphical Abstract

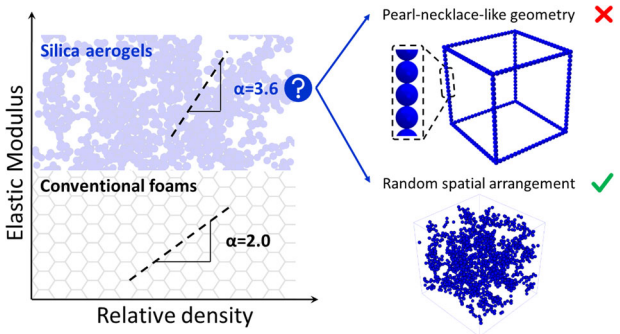

Keywords Silica aerogels · Pore-wall morphology · Particle spatial arrangement · Random network connectivity · Scaling exponents

Highlights

- Presents a microstructure-informed model to study mechanics of silica aerogels.
- Views a fundamental issue of the scaling exponent in power law relations.
- Accounts for the effect of pearl-necklace-like cell walls.
- Describes the random spatial arrangement of the aerogel network using a DLCA model.

✉ Ameya Rege
ameya.rege@dlr.de

[1] Institute of Materials Research, German Aerospace Center (DLR), Cologne, Germany

[2] Department of Chemistry, University of Cologne, Cologne, Germany

[3] School of Computer Science and Mathematics, Keele University, Staffordshire, UK

Published online: 26 June 2023

1 Introduction

Silica aerogels represent a class of nanoporous materials with an unusual combination of properties such as ultralow density (0.003 g/cm^3) and large specific surface areas (in the order of 1000 m^2/g) resulting from their highly mesoporous structure resulting in very low thermal conductivity (less than 0.015 W/mK) [1]. These properties make silica aerogels suitable for numerous applications such as acoustic and thermal insulators, drug delivery, cosmetics, (bio)catalysis, Cherenkov detectors, Knudsen pumps and construction applications as well as space applications [2]. The potential applications of silica aerogels with engineered properties has manifested in an increased research on the accurate understanding of their unique structure-property relationships. Within this context, the mechanical structure-property relations become very interesting because silica aerogels are classically known to be brittle materials. Several chemical and physical modifications have shown to be successful in synthesizing silica-based aerogels with high strength and high flexibility [3–6]. One significant property that is used to quantify the properties in (silica) aerogels is their density [7]. This can be achieved, for e.g., by applying power scaling relations. A classical example of such a relation is $E \propto \rho^{\alpha}$ or $\lambda_s \propto \rho^{\beta}$, where E, λ_s and ρ represent the elastic modulus, solid thermal conductivity, and density of the material while α and β are exponents resulting from the power scaling [8, 9]. In the case of silica aerogels, the exponent α falls between 3–4 [10, 11]. Woignier et al. [11] suggested that the pore volume and the spatial arrangement of the particles may be possible factors responsible for the scaling relation of their elastic properties. While it may prove challenging to critically investigate the reasons at the morphological level, computational approaches may be utilized to design a detailed study.

Gibson and Ashby [12] showed analytically that the scaling exponent in the case of foam-like ideally connected open-cellular materials would be 2. This is found to be true for many experimentally-tested foam-like materials [13], as well as some aerogels, particularly those from biopolymers, owing to their foam-like network architecture [14]. This was computationally justified in a recent study [15]. Rege et al. [16] demonstrated the effect of pore-size distributions on the mechanical properties of open-porous cellular materials within the framework of a constitutive model. This study was further extended by accounting for the influence of the pore space on the elastic properties of open-porous material [17]. It was shown that while density is a critical and significant factor controlling the quantification of their mechanical properties, the role of pore-size distributions and pore-wall thickness cannot be neglected.

In contrast to conventional foam-like materials, silica aerogels typically exhibit a scaling exponent between 3 and 4. This poses a question: What really affects this scaling relation in silica aerogels? To the best of the knowledge of the authors, there seem to arise three factors that may eventually control the scaling relationships, particularly for their elastic properties. These are the randomness in the spatial arrangement or network connectivity of the particles through the aerogel network, the amount of dangling mass, and the pearl-necklace-like morphology of the pore walls. It seems feasible to investigate these three features at a computational level. This can be realized by modeling silica aerogels and simulating their mechanical behavior.

A perspective on the applicability of the different modeling and computational reconstruction approaches for a variety of aerogels was recently reported by Rege [18]. In particular, the morphology of silica aerogels can be well described by aggregation algorithms [19–21]. Here, the diffusion-limited cluster-cluster aggregation (DLCA) or the ballistic aggregation algorithms have been applied. Such models account for the random spatial arrangement of the particles in the aerogel network. While, these models are merely mathematical constructs, they can be used to describe the mechanical properties of aerogels as described in previous reports [21, 22], however, this will be discussed in greater detail in subsequent sections. Within the context of spatial arrangement, the concept of a backbone becomes predominantly interesting. Colloid-like material networks exhibit a critical backbone path within the material's network that bears the majority of the load being transmitted through the material. The remaining network paths remain nearly stress-free. This was shown to be the case in aerogels too [21]. Furthermore, the role of dangling mass toward the power-scaling relation was an interesting subject and has already been intensively investigated by Ma et al. [22] who illustrated that the dangling mass plays no role in the scaling behavior in aerogels. The final feature that may be responsible for the scaling relation is the pearl-necklace-like morphology. This was initially investigated by Woignier et al. [23] on the basis of a unit cell model, whose edges were described as arrays of spheres with no overlap. In a subsequent report, the effect of overlap was analyzed by Morales-Florez et al. [24], where they described the silica aerogel morphology as hierarchical overlapped particle clusters and studied the effect of the overlapped volume on the mechanical properties. They particularly focused on the influence of these overlaps and the subsequent change in porosity on the resulting tensile strength. By accounting for the overlaps, the effect of varying neck sizes on the axial, bending and buckling behavior of the pore walls was recently investigated by Rege et al. [25]. Large deviations resulting from varying the particle overlaps were observed. The model was further improved to account for accurately describing a particle neck and the improvised model was numerically and computationally exploited to characterize

the mechanical properties of silica aerogels [26]. Given the importance to the subject in the literature, it seems feasible to investigate the effect of particle necking on the scaling relation.

Unfortunately, due to the mesoporous nature of the silica aerogel morphology, there have been no experimentally-driven concluding remarks on the origins of this unusual scaling exponents. However, with the effect of dangling mass being negated with computational investigations, the effect of two structural features, viz., the randomness in the spatial arrangement and the inter-particle necks on the scaling exponent has yet to be extensively analyzed. Thus, the effect of the pore-wall structure and the random network connectivity are independently investigated in the following sections.

2 Effect of pore-wall morphology

The effect of the corrugated pore-structure is investigated as an extension of the open-cell foam model proposed by Gibson and Ashby [12]. Lei and Liu [27] also developed a finite element model for silica aerogels by accounting for the dangling mass but not the pearl-necklace-like morphology. While they could show that the dangling mass did not have an effect on the scaling exponent for the elastic modulus, the model assumed constant cross-section of the pore-walls and the effects resulting from such corrugations were not accounted and the model simply resulted in an exponent of 2.04. In the following, a model describing the relations between the elastic properties and the density in the form of scaling laws is demonstrated. The effect of accounting for the pearl-necklace-like morphology of the pore-wall structure on the mechanical properties has been recently studied by our group [25, 26] and in this work, we have integrated the corrugated pore-wall morphology within the unit cell model to study their influence on the scaling of the elastic properties (see Fig. 1).

The degree of the corrugation can be expressed in terms of the neck size. As seen in Fig. 1, the smaller the neck size ($2x$ in terms of the diameter), the more corrugated the pore-wall appears. In this study, we use five different neck sizes which are a function of the particle radius (0.4R, 0.8R, 1.2R, 1.6R, 2R) and five different t/L ratios (0.05, 0.045, 0.04, 0.035, 0.03) corresponding to five different solid

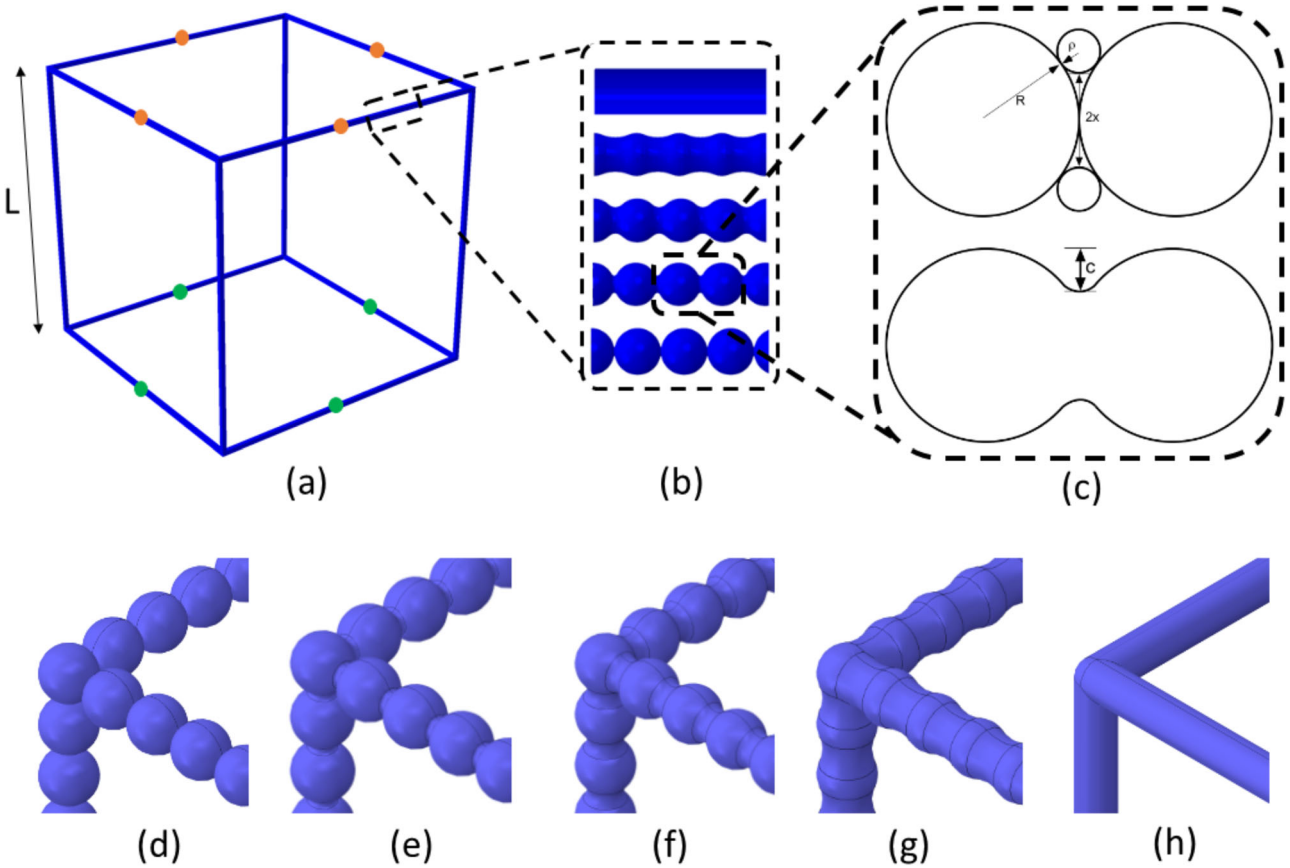

Fig. 1 **a** Unit cell, **b** with corrugated pore-walls, **c** geometric model describing the model of inter-particle necks (figure reused from Ratke et al. [26]), Corners of the corrugated unit cell for neck sizes, **d** 0.4R, **e** 0.8R, **f** 1.2R, **g** 1.6R, **h** 2R

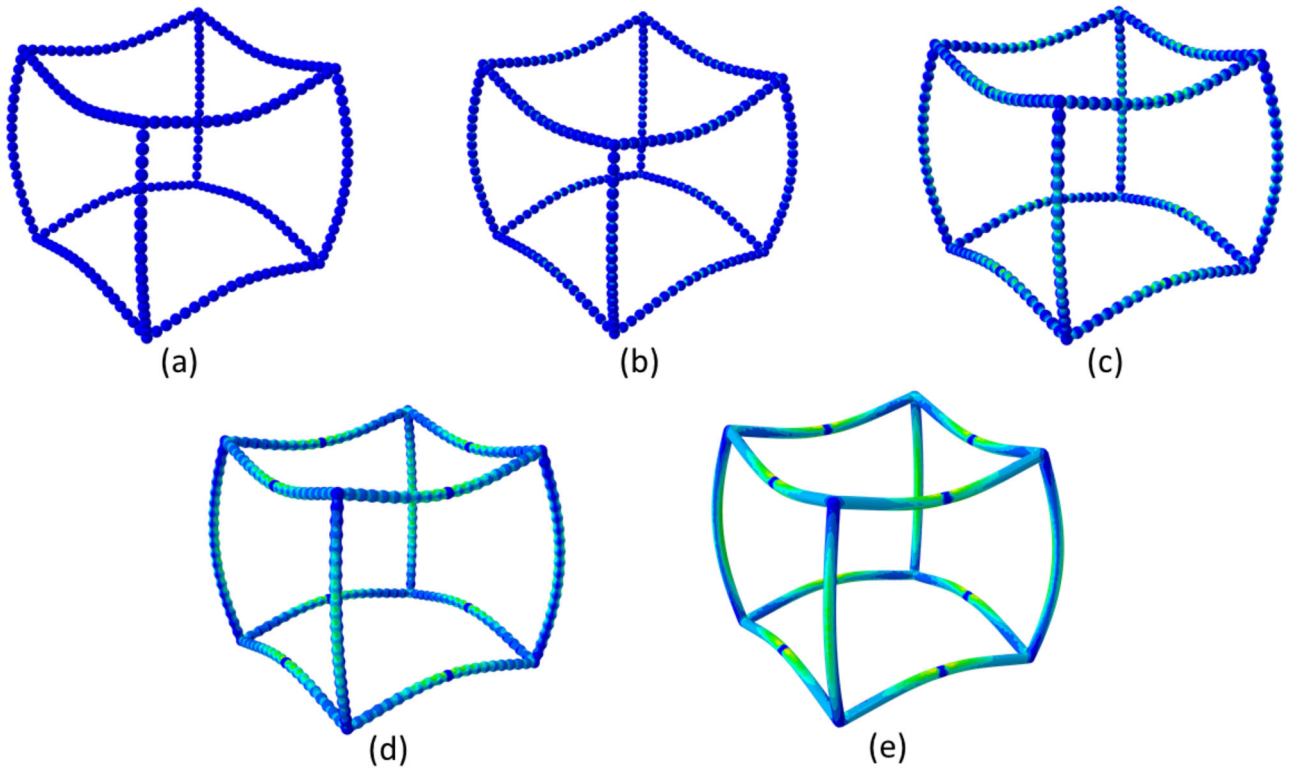

Fig. 2 Deformation of unit cells for neck sizes, **a** 0.4R, **b** 0.8R, **c** 1.2R, **d** 1.6R, **e** 2R

fractions. Here, t denotes the effective diameter and L the length of the pore-wall. The last case, in which the neck size is equal to the particle diameter, corresponds to the case of simulating the pore-wall with constant cross-section. This serves as a benchmark to compare the effect of the corrugations. Since the pore-walls are simulated as slender beams, only the corners of the unit cell are visualized in Fig. 1d–h. The geometry of the neck can be modeled in 2D as shown in Fig. 1c, essentially as a fillet with tangent continuity before transforming to 3D geometry.

All the finite element simulations presented to investigate the influence of the pore corrugations were performed using Abaqus. A single unit cell in accordance with the Gibson-Ashby model [12] was considered to effectively compare the results (influence of the pore corrugations on scaling exponents). The unit cells are compressed up to 20% and the Young's modulus is obtained from the slope of the stress-strain curve in the elastic region. This is simulated as a displacement-driven problem with concentrated loads and point supports (see Fig. 1) in accordance with the open-cell foam model [12]. The deformation of the unit cells is depicted in Fig. 2. It is observed that for larger particle necks, i.e., lower degree of corrugations, the stresses are uniformly distributed and homogeneous while in case of smaller particle necks corresponding to higher degree of corrugations, there are stress concentrations at the necks which can be expected considering elementary mechanics. These stress concentrations at the particle necks could be a reason for the brittle nature of fracture in such materials.

Furthermore, to correlate the structural features of the unit cells with their material properties, we obtain the scaling exponents for the Young's modulus vs. density power law, $E \propto \rho^{\alpha}$. This scaling law can be expressed in terms of the bulk $(.)_b$ and skeletal $(.)_s$ properties as:

$$\frac{E_b}{E_s} \propto \left(\frac{\rho_b}{\rho_s}\right)^{\alpha}, \tag{1}$$

where the bulk properties correspond to the unit cell while the skeletal properties correspond to the individual beams constituting the unit cell. The relative density can be expressed in terms of the geometrical features of the unit cell. Since the mass is the same for skeletal and bulk density, the ratio of the densities is obtained from the ratio of the volumes as follows:

$$\frac{\rho_b}{\rho_s} = \frac{V_s}{V_b}, \tag{2}$$

where V_s is the skeletal volume corresponding to the cell walls and V_b is the bulk volume corresponding to the unit

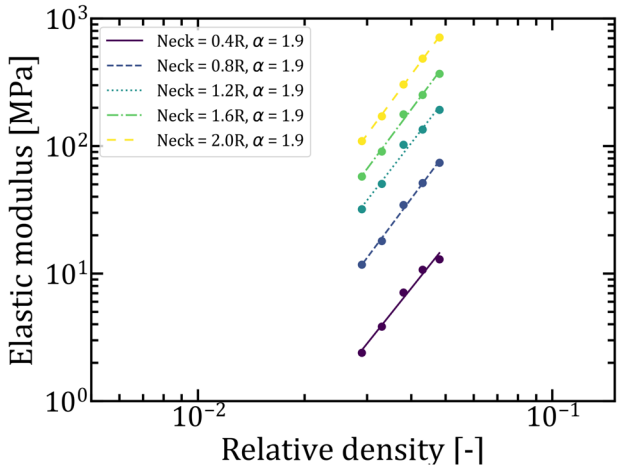

Fig. 3 Scaling exponent for the unit cell model with varying neck sizes under compression

cell. Thus:

$$\frac{\rho_b}{\rho_s} = C\left(\frac{t}{L}\right)^2. \tag{3}$$

Considering the geometry, the constant C can be obtained and the densities can be correlated to the t/L ratio.

The scaling exponents α are obtained for the five different particle neck sizes considered and are illustrated in Fig. 3. It is observed that the deviations in the scaling exponent (1.9 ± 0.03) due to the considerations of the corrugated pore wall are rather insignificant and these marginal differences do not follow any specific trend. Thus, it can be concluded that the inter-particle necks purely do not affect the scaling relationship between the elastic modulus and the density. Of course, as can be visualized from Fig. 2, the stress distribution varies largely and thus, these necks will strongly have an effect on the deformation and mode of failure of the material. The effect of these neck-sizes on the maximal axial and bending stresses and the critical buckling load have been previously reported [25]. However, within the context of the exponent, it seems to be not influential. Moreover, an exponent of nearly 2 is obtained for all the simulated cases. This primarily implies that the pore-wall corrugations do not contribute to the high scaling exponent observed in the case of silica aerogels.

3 Effect of random spatial arrangement of particles

It can now be established that neither the pore-wall morphology nor the dangling mass contribute toward the high scaling exponent in silica aerogels. Thus, it must ultimately lie with the effect of the spatial arrangement of the particles through the aerogel network. This spatial arrangement for silica aerogels can be described by their Hausdorff or fractal dimension. Silica aerogels have been reported to exhibit a fractal morphology [28]. Models based on DLCA have successfully demonstrated this feature [19, 21]. The more dense the aerogels, the higher is their fractal dimension [21]. However, the fractal dimension does not alone uniquely define structural features in silica aerogels [29]. Owing to previously established successful validations between experimental and computational results, we have applied the DLCA algorithm to model silica aerogels. The algorithm is a numerical simulation of the aggregation resulting from the sol-gel process that takes place during the gelation of the silica gel network. Unlike the diffusion limited aggregation (DLA) models, the DLCA takes into account the cluster-cluster aggregation as per the Smoluchowski theory [30], thus providing a better numerical algorithm to model the chemical kinetics behind the gelation process. In some previous works, the DLCA has been applied to model the structural morphology and also the mechanical properties of silica aerogels with reasonable accuracy [19, 21]. For this study, the DLCA algorithm as developed by Meakin and Family [31] was applied. The DLCA algorithm generates a representative volume element (RVE) for further simulations and has four model parameters: the relative density of the RVE (ϱ), the radius of particles (r), the step size of the particles (u) and the domain size (L). The relative density of the RVE can calculated as:

$$\varrho = N\frac{4\pi r^3}{3L^3}, \tag{4}$$

where N is the number of particles in the system. The particles undergo a spherical random walk periodically, given by the equation:

$$\begin{aligned} x_{\text{new}_i} &= x_{\text{old}_i} + u_i \cos\phi \sin\theta, \\ y_{\text{new}_i} &= y_{\text{old}_i} + u_i \sin\phi \sin\theta, \\ z_{\text{new}_i} &= z_{\text{old}_i} + u_i \cos\theta, \end{aligned} \tag{5}$$

where x_i, y_i and z_i are the coordinates of the ith particle in the cluster, and ϕ and θ are the spherical angles selected randomly. For the given study, particles of radius $r = 2$ nm were randomly initiated in a domain of size $L = 300$ nm. The particles move randomly with a step size $u = 1$ nm per unit time. On initialization of the algorithm, when two particles come within a critical distance of each other, defined by $\epsilon = 2.15 \times r$, the two particles aggregate to form a cluster. The simulation continues till there is only one connected cluster left in the RVE, resulting in the silica aerogel microstructure, as visualized in Fig. 4a.

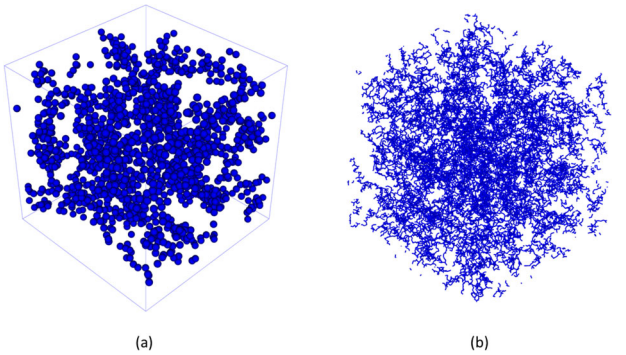

Fig. 4 **a** Exemplary particle-aggregated network generated using DLCA algorithm with fewer number of particles illustrating the particle-aggregated morphology as observed in silica aerogels, **b** the exported network of bonds from the actual model simulated in the finite element program with 24,171 particles

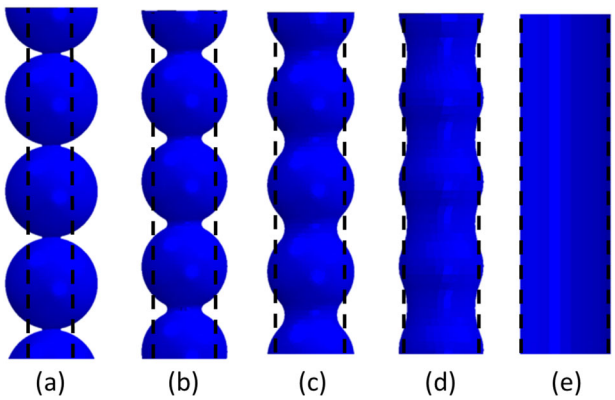

Fig. 5 Effective diameter for considering the pore-structure with different neck sizes, **a** 0.4R, **b** 0.8R, **c** 1.2R, **d** 1.6R, **e** 2R

In this study, we define four structures generated by implementing the DLCA approach with four different relative densities, viz. 0.03, 0.04, 0.05, and 0.06. These structures are compressed up to 10% strain in an uniaxial compressive mode of deformation, and the elastic modulus is obtained from the slope of the stress-strain curve of the elastic region. The aggregated particle positions obtained from the DLCA algorithm are exported to a finite element program. The connections between the particle centers were modeled as a bond with a length of $2.15 \times r$. To capture all the modes of deformation undergoing in a particle bond, viz. torsion, bending and axial stretching, these particle bonds were simulated as beam elements with the finite element program Abaqus. Hence, the bond (beam) diameter is the only geometrical input for the simulation other than the structure itself.

Although the pore-wall morphology was shown to have a negligible effect on the scaling exponent, we include different neck sizes while simulating the DLCA structures for completeness. This is achieved by using an effective beam diameter calculated based on volume balance for the particle bonds. This

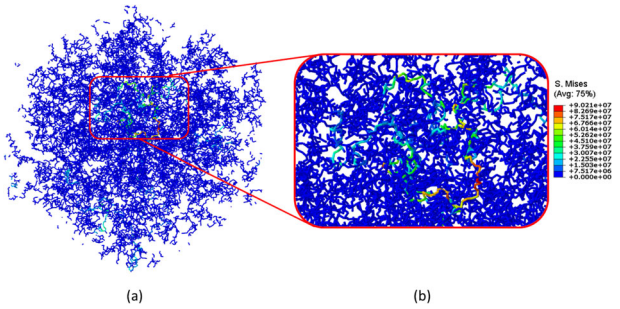

Fig. 6 Deformation of the simulated DLCA-based silica aerogel model. **a** Deformed RVE demonstrating nearly the entire network remaining stress-free under 10% uniaxial compression and **b** zoomed part of the load-bearing backbone paths in model silica aerogels showing high stress-concentrations

effective diameter is obtained such that the volume of the constant cross-section it represents is equal to the volume of the corresponding corrugated pore-wall with the given neck size (see Fig. 5). The deformation of one of the RVEs under compressive stresses can be visualized in Fig. 6. The undeformed RVE shown in Fig. 4b corresponds to a relative density of 0.03 and 24,171 particles are aggregated using the DLCA algorithm. Under uniaxial compression, while a majority of the RVE remains stress-free (comparing Figs. 4b and 6a) even at 10% compression, the stresses are transmitted through the skeletal backbone chain (Fig. 6b). This, as described previously, is the critical load-bearing path typically known from colloidal mechanics. This trend of backbone-path-formation in silica aerogels was also previously reported [21].

The scaling exponent is calculated for the five different neck sizes (in the form of effective diameter) considered in the previous section for the four different DLCA structures and is illustrated in Fig. 7. It can be observed that the scaling exponent is nearly 3.6 irrespective of the neck-size considered. Before drawing a conclusion, a short remark: Note that while an effective diameter is considered, it eventually models a constant cross-section of the simulated beams. This indicates that the random network connectivity is the primary reason for an unusual scaling exponent in the case of silica aerogels.

To further scrutinize this conclusion, we add one more parameter to the model. In the above-mentioned model, the effective diameter was assumed constant throughout a given simulated microstructure. In reality, it is highly improbable that all the neck sizes of the particle-aggregated structures will be exactly the same. Thus, we explored the use of a distribution of neck sizes for any given DLCA structure. For simplicity, we considered three very coarse normal distributions as shown in Fig. 8 with different mean neck sizes. The particle bonds simulated as beams were divided into five sets of different beam diameters depending upon their frequency. Thus, DLCA structures with different neck sizes and beam diameters were simulated. This approach can be further extended for finer distributions for enhanced accuracy of the results.

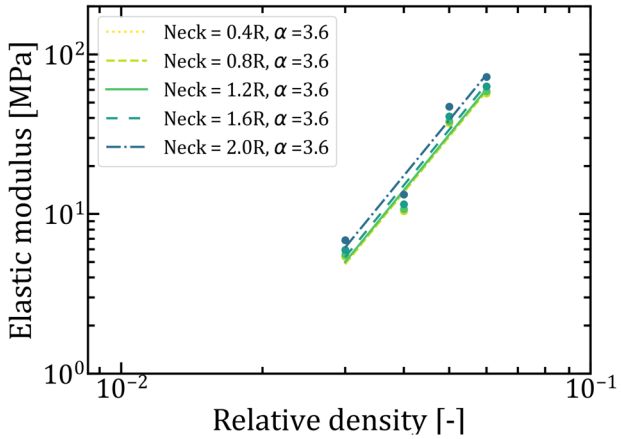

Fig. 7 Scaling exponent for DLCA structures with different effective neck sizes

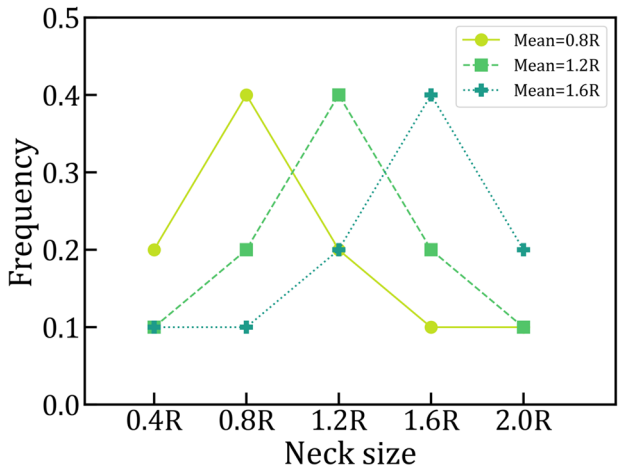

Fig. 8 Distribution of neck sizes with different mean neck sizes

The DLCA structures were simulated with each of the three distributions and the scaling exponents were obtained. The scaling exponent for the different distribution of the neck sizes was also found to be close to 3.6 (see Fig. 9). Thus, even the particle neck-size distributions do not influence the scaling exponent. It may thus be said with reasonable accuracy that the driving factor behind the power-scaling exponent is the random spatial arrangement of the particles, i.e., the network connectivity. This does not exclude the possibility of further parameters that may be additionally responsible for the scaling relation, however, since the random network connectivity precisely predicts the exponent, it may certainly be established as the primary factor.

4 Conclusions

In this paper, the origin of the scaling exponent between the elastic modulus and density in the case of silica aerogels has been investigated in a heuristic manner. Three factors, viz., the pore-wall morphology, the random spatial arrangement of particles in the aerogel network, and the dangling mass, are proposed as possible physical aspects responsible for the high scaling exponent in silica aerogels. However, since the effect of the dangling mass has been negated by previous studies, a detailed computational investigation has been presented considering the effect of the pore-wall morphology within the framework of the unit cell model and the effect of the random spatial arrangement of particles. Based on the results from this study, it may be concluded that the pore-wall morphology, i.e., the pearl-necklace-like structure of the pore walls, has nearly no effect on the scaling exponent. Changing the inter-particle neck sizes also shows no significant changes in the exponent. However, accounting for the random network connectivity, within the framework of a DLCA model, directly results in an exponent of 3.6, which is in good agreement with previous experimental results. Adding the effect of constant or a distribution of inter-particle neck sizes shows no further changes in the exponent. It can thus be established that the random spatial arrangement of particles in the aerogel network is the primary reason behind the origin of the scaling exponent within the context of the relation between the elastic modulus and density in the case of silica aerogels.

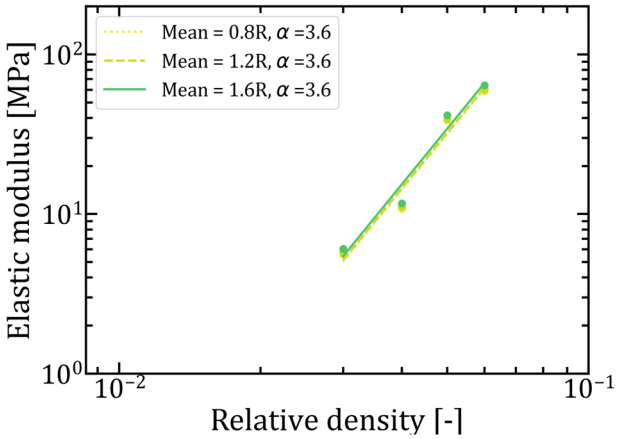

Fig. 9 Scaling exponent for DLCA structures with different neck size distributions

Funding Open Access funding enabled and organized by Projekt DEAL.

Compliance with ethical standards

Conflict of interest The authors declare no competing interests.

Publisher's note Springer Nature remains neutral with regard to jurisdictional claims in published maps and institutional affiliations.

References

1. Pierre AC, Rigacci A (2011) SiO2 aerogels. Springer, New York, NY, p 21–45
2. Smirnova I, Gurikov P (2017) Aerogels in chemical engineering: strategies toward tailor-made aerogels. Annu Rev Chem Biomol Eng 8:307–334
3. Leventis N, Sotiriou-Leventis C, Zhang G, Rawashdeh A-MM (2002) Nanoengineering strong silica aerogels. Nano Lett 2:957–960
4. Rao AV, Bhagat SD, Hirashima H, Pajonk G (2006) Synthesis of flexible silica aerogels using methyltrimethoxysilane (mtms) precursor. J Colloid Interface Sci 300:279–285
5. Maleki H, Durães L, Portugal A (2014) An overview on silica aerogels synthesis and different mechanical reinforcing strategies. J Non Cryst Solids 385:55–74
6. Zu G et al. (2018) Versatile double-cross-linking approach to transparent, machinable, supercompressible, highly bendable aerogel thermal superinsulators. Chem Mater 30:2759–2770
7. Wong JCH, Kaymak H, Brunner S, Koebel MM (2014) Mechanical properties of monolithic silica aerogels made from polyethoxydisiloxanes. Microporous Mesoporous Mater 183:23–29
8. Lemay JD (1990) Mechanical structure-property relationships of microcellular, low density foams. MRS Online Proceedings Library (OPL), vol 207, p 21
9. Weigold L, Reichenauer G (2014) Correlation between mechanical stiffness and thermal transport along the solid framework of a uniaxially compressed polyurea aerogel. J Non Cryst Solids 406:73–78
10. Groß J, Fricke J (1995) Scaling of elastic properties in highly porous nanostructured aerogels. Nanostruct Mater 6:905–908
11. Woignier T, Phalippou J, Vacher R (1989) Parameters affecting elastic properties of silica aerogels. J Mater Res 4:688–692
12. Gibson I, Ashby MF (1982) The mechanics of three-dimensional cellular materials. Proc R Soc Lond A Math Phys Sci 382:43–59
13. Gibson LJ, Ashby MF (1999) Cellular solids: structure and properties. Cambridge University Press, Cambridge, United Kingdom
14. Zhao S, Malfait WJ, Guerrero-Alburquerque N, Koebel MM, Nyström G (2018) Biopolymer aerogels and foams: chemistry, properties, and applications. Angew Chem Int Ed 57:7850–7608
15. Chandrasekaran R et al. (2021) Computational design of biopolymer aerogels and predictive modelling of their nanostructure and mechanical behaviour. Sci Rep 11:10198
16. Rege A, Aney S, Milow B (2021) Influence of pore-size distributions and pore-wall mechanics on the mechanical behavior of cellular solids like aerogels. Phys Rev E 103:043001
17. Aney S, Rege A (2023) The effect of pore sizes on the elastic behaviour of open-porous cellular materials. Math Mech Solids 28:1624–1634
18. Rege A (2023) A perspective on methods to computationally design the morphology of aerogels. Adv Eng Mater 25:2201097
19. Hasmy A, Foret M, Pelous J, Jullien R (1993) Small-angle neutron-scattering investigation of short-range correlations in fractal aerogels: simulations and experiments. Phys Rev B 48:9345–9353
20. Grzegorczyk M, Rybaczuk M, Maruszewski K (2004) Ballistic aggregation: an alternative approach to modeling of silica sol-gel structures. Chaos Solitons Fractals 19:1003–1011
21. Abdusalamov R et al. (2021) Modeling and simulation of the aggregation and the structural and mechanical properties of silica aerogels. J Phys Chem B 125:1944–1950
22. Ma H, Roberts A, Prévost J, Jullien R, Scherer G (2000) Mechanical structure-property relationship of aerogels. J Non Cryst Solids 277:127–141
23. Woignier T, Phalippou J (1988) Mechanical strength of silica aerogels. J Non Cryst Solids 100:404–408
24. Morales-Flórez V, Rosa-Fox NDL, Piñero M, Esquivias L (2005) The cluster model: a simulation of the aerogel structure as a hierarchically-ordered arrangement of randomly packed spheres. J Sol Gel Sci Technol 35:203–210
25. Rege A, Aney S, Ratke L (2022) Impact of pearl-necklace-like skeleton on pore sizes and mechanical properties of porous materials: a theoretical view. AIP Adv 12:105108
26. Ratke L, Rege A, Aney S (2022) The effect of particle necks on the mechanical properties of aerogels. Materials 16:230
27. Lei J, Liu Z (2018) A novel constitutive model for the mechanical properties of silica aerogels. J Appl Phys 124:025102
28. Lours T, Zarzycki J, Craievich AF, Aegerter MA (1990) Textural characteristics of silica aerogels from saxs experiments. J Non Cryst Solids 121:216–220
29. Abdusalamov R, Pandit P, Milow B, Itskov M, Rege A (2021) Machine learning-based structure-property predictions in silica aerogels. Soft Matter 17:7350–7358
30. Smoluchowski MV (1916) Drei Vortrage uber Diffusion, Brownsche Bewegung und Koagulation von Kolloidteilchen. Zeitschrift fur Physik 17:557–585
31. Meakin P, Family F (1988) Structure and kinetics of reaction-limited aggregation. Phys Rev A 38:2110–2123